

Article

Boninites in the ~3.3 Ga Holenarsipur Greenstone Belt, Western Dharwar Craton, India

Tarun C. Khanna ^{1,*}, V. V. Sessa Sai ², S. H. Jaffri ¹, A. Keshav Krishna ¹ and M. M. Korakoppa ²

¹ CSIR-National Geophysical Research Institute, Telangana, Hyderabad 500007, India; syed1401@rediffmail.com (S.H.J.); keshav_aradhi@rediffmail.com (A.K.K.)

² Geological Survey of India, Bandlaguda, Hyderabad 500068, India; seshu1967@gmail.com (V.V.S.S.); seshubb@yahoo.co.in (M.M.K.)

* Correspondence: khannangri@ngri.res.in or khannangri@gmail.com; Tel.: +91-98-4824-0367

Received: 31 May 2018; Accepted: 3 July 2018; Published: 5 July 2018



Abstract: In this contribution, we present detailed field, petrography, mineral chemistry, and geochemistry of newly identified high-Si high-Mg metavolcanic rocks from the southern part of the ~3.3 Ga Holenarsipur greenstone belt in the western Dharwar craton, India. The rocks occur as conformable bands that were interleaved with the mafic-ultramafic units. The entire volcanic package exhibits uniform foliation pattern, and metamorphosed under greenschist to low grade amphibolite facies conditions. The rocks are extremely fine grained and exhibit relict primary igneous textures. They are composed of orthopyroxene and clinopyroxene phenocrysts with serpentine, talc, and amphibole (altered clinopyroxene). Cr-spinel, rutile, ilmenite, and apatite occur as disseminated minute grains in the groundmass. The mineralogical composition and the geochemical signatures comprising of high SiO₂ (~53 wt. %), Mg# (~83), low TiO₂ (~0.18 wt. %), and higher than chondritic Al₂O₃/TiO₂ ratio (~26), reversely fractionated heavy rare earth elements (REE) (Gd_N/Yb_N ~0.8), resulting in concave-up patterns, and positive Zr anomaly, typically resembled with the Phanerozoic boninites. Depletion in the high field strength elements Nb, and Ti relative to Th and the REE in a primitive mantle normalized trace element variation diagram, cannot account for contamination by pre-existing Mesoarchean continental crust present in the study area. The trace element attributes instead suggest an intraoceanic subduction-related tectonic setting for the genesis of these rocks. Accordingly, the Holenarsipur high-Si high-Mg metavolcanic rocks have been identified as boninites. It importantly indicates that the geodynamic process involved in the generation of Archean boninites, was perhaps not significantly different from the widely recognized two-stage melt generation process that produced the Phanerozoic boninites, and hence provides compelling evidence for the onset of Phanerozoic type plate tectonic processes by at least ~3.3 Ga, in the Earth's evolutionary history.

Keywords: boninite; komatiite; Mesoarchean; Holenarsipur; Dharwar craton; India

1. Introduction

Boninites, and boninite-series volcanic rocks have been widely recognized in the Phanerozoic intraoceanic arc systems [1,2], and the Ophiolites, [3,4]. They are produced by the partial melting of a prior depleted refractory mantle wedge, metasomatized by subducted slab-derived fluids during the initial stages of the melt generation process. Their reported occurrence in the Archean greenstone successions is not very extensive. Nevertheless, there are some classical examples of boninitic magmatism that has been identified in the ~3.7 Ga Eoarchean [5], ~3.1 Ga Mesoarchean [6], and the ~2.7 Ga Neoarchean [7,8] greenstone terranes.

In this contribution, we present detailed field, petrography, and geochemistry of the newly identified high-Si high-Mg volcanic rocks from one of the oldest supracrustal sequences of late

Paleoarchean age in the Dharwar craton, India. The rocks exhibit typical boninite geochemical fingerprints and they occur within the southern part of the ~3.3 Ga Holenarsipur greenstone belt [9] in the western sector of the Dharwar craton (Figure 1). This new finding essentially bridges the gap between the late Eoarchean [5] and the early Mesoarchean [6], and it provides convincing evidence for the persistence of subduction-related plate tectonic processes throughout the Archean during the Earth's early evolutionary history.

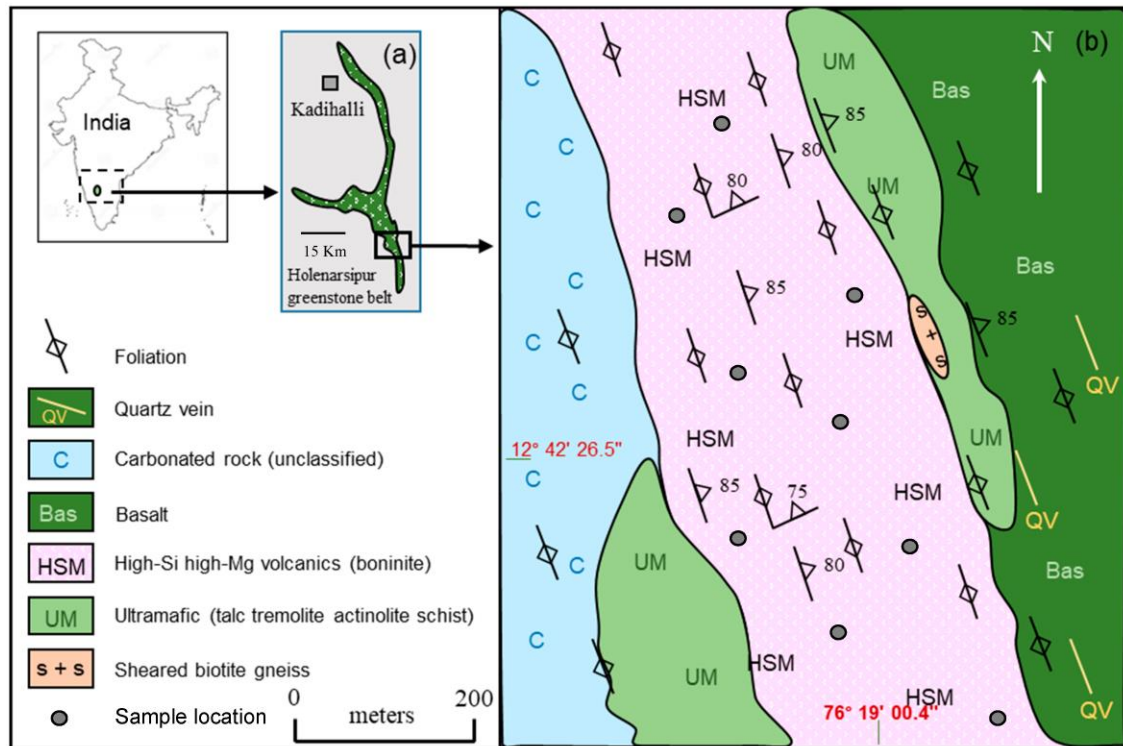


Figure 1. An outline map of India showing: (a) the location of the Holenarsipur greenstone belt in the western Dharwar craton; and, (b) detailed geological map of the study area located in the south of the Holenarsipur greenstone belt.

2. Regional Geology

The Dharwar proto-continent is subdivided into three distinct cratonic blocks: the western Dharwar craton, the eastern Dharwar craton, and the southern granulite terrane [10]. The western and eastern sectors of the Dharwar craton comprise of laterally extensive and linearly arcuate Mesoarchean and Neoarchean greenstone terranes surrounded by gneisses and granitoids. The NNW–SSE trending shear zone, extending along the eastern margin of the Chitradurga greenstone belt [11], separates the eastern greenstone belts from those in the western sector of the Dharwar craton.

The study area, the Holenarsipur greenstone belt (Figure 1a), is one of the oldest supracrustal belts in the western Dharwar craton, India. It has a strike length of about 70 km in the N–S direction. It consists of mafic-ultramafic, felsic volcanic rocks, and sedimentary units. Lithologies in the belt were subjected to greenschist to low grade amphibolite facie metamorphism. A metarhyolite flow from the northern part of the belt yielded a sensitive high-resolution ion microprobe (SHRIMP) U–Pb zircon age of 3.298 ± 0.007 Ga [9]. For further reading on the geological aspects of the Holenarsipur belt and the surrounding gneisses, the reader is referred to previous publications [9–12].

The focus of this study is the metavolcanic unit exposed in the southern part of the greenstone belt (Figure 1a,b). Underneath the weathered surface of the outcrop, the rock is relatively fresh and melanocratic in appearance, with well-developed planar fabric (Figure 2a). The rocks are exposed as low lying linear outcrops with an undulated topography. They are conformably juxtaposed with

magnetite bearing metaultramafic rocks (Figure 2b) and metabasalts (Figure 2c). Collectively, the rocks exhibit uniform and identical foliation patterns. The major foliation is vertical and trends in the NNW–SSE direction. At few places the foliation exhibits steep subvertical dips of 85° towards east. A second set of deformation fabric trending ENE–WSW with steep northerly dip of 75° is also noticed. Minor oval shaped outcrop of sheared biotite granite gneiss is noticed along the contact between the high-Si high-Mg volcanics and the metaultramafic rocks (Figure 1b). NNW–SSE trending folds are also noticed in the adjacent metaultramafics (Figure 2d). The folds are northerly plunging with an axial plane dip of 75° towards west. The unclassified carbonated rocks occur to the west of this unit, while the amphibolites (arc tholeiites) occur to the east. Minor enclaves of older Tonalite–Trondhjemite–Granodiorite (TTG) gneisses and metaultramafics occur as linear bodies that are juxtaposed along the contact of boninitic rocks and the amphibolite. On the basis of highly deformed nature of the TTG gneiss patches and the metaultramafics and their disposition in the field, we infer that these are the caught-up patches of the older material.



Figure 2. Field photograph of (a) high-Si high-Mg volcanics (boninite) that are relatively fresh and greyish in appearance underneath the weathered surface of the outcrop; (b) magnetite bearing metaultramafic rocks conformably juxtaposed with the high-Si high-Mg volcanics; (c) amphibolites (metabasalts) are conformably associated with the adjacent ultramafics; (d) second generation (F2) folds observed in the adjacent ultramafic outcrop. Note that, as shown in Figure 1, the entire volcanic package exhibits uniform foliation pattern, and consistent grade of metamorphism.

3. Sampling and Analytical Methods

The samples were collected from the southern part of the Holenarsipur greenstone belt (Figure 1a,b; N $12^\circ 42' 26.5''$; E $76^\circ 19' 00.4''$). The rocks are fine grained and greyish black in appearance. Nine representative samples were collected from relatively fresh portions of the outcrop devoid of quartz veins and secondary mineralization. The samples were further processed for bulk-rock major

and trace element geochemistry. For the purpose of comparison between the interelement relationships, representative geochemical composition of a spinifex textured komatiite, which occurs as an ultramafic enclave in the gneisses, near Kadihalli (Figure 1a; N 13°10'05.4"; E 76°11'16.0") [13], which is located ~50 km north of the study area, is also presented in this paper.

The mineral compositions were determined by electron probe microanalysis on a CAMECA SX-100 (CAMECA SAS, Gennevilliers CEDEX, France) at the Petrology Division, Geological Survey of India, Hyderabad, India. A 20 nA beam current and an accelerating voltage of 15 keV were maintained with a focused beam. Certified natural silicate standards (supplied by P&H, UK) were used for the instrument calibration. The corrections for ZAF were applied online by the instrument software. The mineral compositions are reported in Tables 1–3.

Table 1. Mineral composition of the clinopyroxene (CPX) and orthopyroxene (OPX) phases present in the Holenarsipur boninites.

	CPX					OPX			
	29/1	30/1	40/1	13/1	38/1	31/1	41/1	47/1	16/1
SiO ₂	54.44	53.91	51.65	52.84	52.94	56.00	53.67	53.82	53.97
TiO ₂	0.16	0.05	0.16	0.22	0.16	0.04	0.12	0.73	0.10
Al ₂ O ₃	0.33	0.68	1.74	4.35	2.88	0.56	3.93	0.87	1.83
Cr ₂ O ₃	0.15	0.12	0.10	0.03	0.10	0.11	0.13	0.03	0.01
FeO ^(T)	3.60	3.72	3.66	11.60	11.35	9.07	10.28	14.12	10.89
MnO	0.08	0.07	0.10	0.30	0.25	0.17	0.31	0.46	0.34
MgO	18.03	17.40	16.94	27.25	29.02	31.87	29.73	27.33	27.36
CaO	23.00	23.32	22.99	0.49	0.60	0.73	1.22	0.67	0.55
Na ₂ O	0.04	0.02	0.00	0.03	0.00	0.01	0.06	0.01	0.03
K ₂ O	0.00	0.00	0.00	0.00	0.00	0.00	0.00	0.00	0.01
NiO	0.00	0.06	0.00	0.02	0.14	0.16	0.06	0.02	0.00
Total	99.85	99.35	97.35	97.11	97.43	98.73	99.50	98.06	95.09
Fe ₂ O ₃	0.26	0.38	1.68	0.00	0.87	0.23	1.35	0.00	0.00
FeO	3.37	3.38	2.15	11.60	10.57	8.86	9.06	14.12	10.89
Total	99.87	99.39	97.52	97.11	97.52	98.75	99.63	98.06	95.09
Number of ions on the basis of 6(O):									
Si	1.98	1.98	1.93	1.92	1.92	1.98	1.90	1.97	2.00
Ti	0.00	0.00	0.00	0.01	0.00	0.00	0.00	0.02	0.00
Al	0.01	0.03	0.08	0.19	0.12	0.02	0.16	0.04	0.08
Cr	0.00	0.00	0.00	0.00	0.00	0.00	0.00	0.00	0.00
Fe ⁺³	0.01	0.01	0.05	0.00	0.02	0.01	0.04	0.00	0.00
Fe ⁺²	0.10	0.10	0.07	0.35	0.32	0.26	0.27	0.43	0.34
Mn	0.00	0.00	0.00	0.01	0.01	0.01	0.01	0.01	0.01
Mg	0.98	0.95	0.94	1.48	1.57	1.68	1.57	1.49	1.51
Ca	0.90	0.92	0.92	0.02	0.02	0.03	0.05	0.03	0.02
Na	0.00	0.00	0.00	0.00	0.00	0.00	0.00	0.00	0.00
K	0.00	0.00	0.00	0.00	0.00	0.00	0.00	0.00	0.00
Ni	0.00	0.00	0.00	0.00	0.00	0.00	0.00	0.00	0.00
Total	4.00	4.00	4.00	3.98	4.00	4.00	4.00	3.99	3.96
Mol.per cent end-members:									
Enstatite (En)	49.21	47.95	47.62	79.50	80.69	84.80	81.35	75.93	80.33
Wollastonite (Wo)	45.14	46.19	46.44	1.03	1.19	1.40	2.41	1.34	1.16
Ferrosilite (Fs)	5.64	5.86	5.94	19.48	18.11	13.80	16.25	22.73	18.51

Table 2. Mineral composition of the amphibole phases present in the Holenarsipur boninites.

	1/1	2/1	3/1	5/1	6/1	7/1	11/1	12/1	14/1	15/1	42/1
SiO ₂	54.48	57.23	57.09	55.80	52.57	51.67	55.93	55.81	56.27	57.33	55.07
TiO ₂	0.21	0.00	0.11	0.15	0.94	0.57	0.10	0.17	0.06	0.01	0.19
Al ₂ O ₃	2.39	0.25	0.32	1.52	2.85	4.30	1.43	0.78	1.12	0.43	2.74
Cr ₂ O ₃	0.79	0.03	0.08	0.35	1.03	0.96	0.49	0.48	0.54	0.09	0.81
Fe ₂ O ₃	2.20	5.34	1.99	2.11	3.45	1.58	2.43	1.34	1.37	1.00	3.44
FeO	1.73	0.00	1.64	2.11	1.64	3.05	1.38	1.97	2.58	2.50	1.24
MnO	0.11	0.19	0.19	0.00	0.11	0.05	0.10	0.00	0.11	0.13	0.03
MgO	20.65	22.61	21.92	21.15	20.10	19.24	21.24	21.69	21.38	21.77	20.70
NiO	0.00	0.00	0.03	0.00	0.13	0.00	0.06	0.04	0.04	0.00	0.00
ZnO	0.00	0.02	0.00	0.06	0.00	0.00	0.10	0.00	0.00	0.16	0.00
CaO	12.45	10.99	12.73	12.66	12.41	12.37	12.55	12.92	13.02	12.93	12.35
Na ₂ O	0.22	0.04	0.02	0.08	0.36	0.50	0.07	0.04	0.07	0.02	0.25
K ₂ O	0.10	0.00	0.01	0.09	0.20	0.26	0.02	0.00	0.02	0.02	0.13
BaO	0.03	0.02	0.00	0.04	0.00	0.04	0.00	0.00	0.02	0.00	0.00
H ₂ O	2.12	2.17	2.15	2.14	2.11	2.08	2.14	2.13	2.15	2.15	2.16
Total	97.47	98.88	98.28	98.25	97.89	96.67	98.04	97.37	98.75	98.52	99.10
Number of ions on the basis of 23(O):											
Si	7.69	7.90	7.95	7.81	7.46	7.43	7.82	7.86	7.84	7.98	7.65
Al ^{iv}	0.31	0.04	0.05	0.19	0.48	0.57	0.18	0.13	0.16	0.02	0.35
Al ^{vi}	0.09	0.00	0.00	0.06	0.00	0.16	0.06	0.00	0.03	0.05	0.10
Ti	0.02	0.00	0.01	0.02	0.10	0.06	0.01	0.02	0.01	0.00	0.02
Cr	0.09	0.00	0.01	0.04	0.12	0.11	0.05	0.05	0.06	0.01	0.09
Fe ³⁺	0.23	0.55	0.21	0.22	0.37	0.17	0.26	0.14	0.14	0.10	0.36
Fe ²⁺	0.20	0.00	0.19	0.25	0.19	0.37	0.16	0.23	0.30	0.29	0.14
Mn	0.01	0.02	0.02	0.00	0.01	0.01	0.01	0.00	0.01	0.02	0.00
Mg	4.35	4.65	4.55	4.41	4.25	4.13	4.43	4.56	4.44	4.52	4.29
Ni	0.00	0.00	0.00	0.00	0.01	0.00	0.01	0.00	0.00	0.00	0.00
Zn	0.00	0.00	0.00	0.01	0.00	0.00	0.01	0.00	0.00	0.02	0.00
Ca	1.88	1.63	1.90	1.90	1.89	1.91	1.88	1.95	1.94	1.93	1.84
Na	0.06	0.01	0.00	0.02	0.10	0.14	0.02	0.01	0.02	0.00	0.07
K	0.02	0.00	0.00	0.02	0.04	0.05	0.00	0.00	0.00	0.00	0.02
Ba	0.00	0.00	0.00	0.00	0.00	0.00	0.00	0.00	0.00	0.00	0.00
Sr	0.00	0.00	0.00	0.00	0.00	0.00	0.00	0.00	0.00	0.00	0.00
Pb	0.00	0.00	0.00	0.00	0.00	0.00	0.00	0.00	0.00	0.00	0.00
F	0.00	0.00	0.00	0.00	0.00	0.00	0.00	0.00	0.00	0.00	0.00
Cl	0.00	0.00	0.00	0.00	0.00	0.00	0.00	0.00	0.00	0.00	0.00
OH	2.00	2.00	2.00	2.00	2.00	2.00	2.00	2.00	2.00	2.00	2.00
Total	16.96	16.81	16.91	16.94	17.02	17.10	16.90	16.96	16.97	16.93	16.93
Comment:	Tremolite	Tremolite	Tremolite	Tremolite	Mg-hornblende	Mg-hornblende	Tremolite	Tremolite	Tremolite	Tremolite	Tremolite

Table 3. Mineral composition of the altered silicates, and the accessory mineral phases present in the Holenarsipur boninites.

	28/1	25/1	32/1	36/1	48/1	49/1
SiO ₂	37.61	60.07	1.50	0.03	0.00	0.01
TiO ₂	0.09	0.13	0.34	0.00	97.30	51.88
Al ₂ O ₃	9.66	0.92	4.83	0.00	0.01	0.00
FeO ^(T)	10.12	3.27	60.96	0.14	0.63	42.95
MnO	0.12	0.02	1.05	0.02	0.00	3.01
MgO	28.90	28.10	0.94	0.13	0.03	0.59
CaO	0.23	1.03	0.44	54.20	0.04	0.01
Na ₂ O	0.06	0.06	0.06	0.00	0.01	0.02
K ₂ O	0.09	0.02	0.00	0.00	0.00	0.00
NiO	0.05	0.03	0.00	0.01	0.00	0.08
ZnO	0.14	0.00	0.06	0.00	0.09	0.00
BaO	0.00	0.00	0.00	0.00	0.83	0.48
Cr ₂ O ₃	0.02	0.10	28.71	0.00	0.55	0.09
ZrO ₂	0.00	0.00	0.00	0.00	0.18	0.00
P ₂ O ₅	0.02	0.07	0.13	43.84	0.00	0.01
Total	87.25	93.88	99.02	99.31	99.67	99.16
Comment:	Serpentine	Talc	Cr-spinel	Apatite	Rutile	Ilmenite

For bulk-rock geochemistry, the rocks were manually powdered using an agate mortar and pestle. Major element oxides (Table 4) were analyzed using fused glass discs, on a Axios mAX wavelength dispersive sequential X-ray fluorescence spectrometer (XRF) (PANalytical, Eindhoven, The Netherlands) coupled with an automatic sample changer and on board instrument software SUPER Q 5.0 (supplied by PANalytical), was used following the method described in [14]. In brief, the fused glass discs for each sample were prepared from a mixture of 2.0 g of the sample/standard with 10.0 g of lithium metaborate:tetraborate (4:1; Spectroflux 100B, United States Alfa Aesar, A Johnson Matthey Company, Ward Hill, MA, USA), using Pt-Au crucibles and molds (Fluxy, Claisse, Laval, QC, Canada).

Trace elements (Table 4) were determined by high resolution inductively coupled plasma mass spectrometry (HR-ICP-MS; Nu Instruments Attom, UK). The procedure is described in [15]. In brief, 50 mg of finely ground sample powder was digested in a freshly prepared mixture of ultrapure HF and HNO₃ at 3:1 ratio, in screw top Teflon “SavilleX” vessels (SavilleX Corporation, Minnesota, USA), and heated on a hot plate at 160 °C. Certified reference material BHVO-1 (supplied by United States Geological Survey, Reston, VA, USA), was dissolved simultaneously and then analyzed along with the samples. Oxide and oxy-hydroxide ratios were low (<0.2%) and the doubly charged ions ratio was <3%. Mass bias fractionation and isobaric interferences were addressed by using certified geochemical reference materials, while the external drift correction was performed by the repeated analyses of BHVO-1. Precision and accuracy are better than the RSD 3% for the majority of the trace elements. The major and trace element concentrations determined for BHVO-1 are in concurrence with the recommended values in the GEOREM database [16]. An independent analysis of international certified reference material BIR-1, (supplied by United States Geological Survey, Reston, VA, USA), which was run as an unknown, and not part of the calibration, is also provided in Table 4.

The selected trace elements are normalized to chondrite and primitive mantle using the values of Sun and Mc Donough [17], and indicated by (N) and (pm) subscripts, respectively. The major element oxides were recalculated to 100% anhydrous for the inter-comparison purpose. The sample powders weighing 1 g each were taken in pure quartz crucibles and heated in a muffle furnace for ~2 h at 900 °C temperature. The loss on ignition values is given in Table 4, which is generally ≤2 wt. %; Mg# is calculated as the mole ratio of Mg/(Mg + Fe²⁺), where Fe²⁺ is assumed to be 90% for the total Fe.

Table 4. Bulk-rock major (wt. %) and trace element (ppm) composition of Holenarsipur boninites and Kadihalli komatiite, western Dharwar craton, India. determined values for BIR-1 are also shown.

	TPK-8	TPK-9	TPK-11	TPK-12	TPK-13	TPK-14	TPK-15	TPK-26	TPK-27	TJK [13]	BIR-1 (%RSD)
SiO ₂	52.62	52.90	53.76	52.44	52.83	52.91	54.47	53.03	53.35	45.10	48.26 (0.72)
TiO ₂	0.15	0.18	0.20	0.17	0.18	0.25	0.16	0.16	0.19	0.30	0.953 (0.52)
Al ₂ O ₃	5.01	4.60	4.82	4.56	4.35	4.69	4.09	4.45	3.90	3.54	15.36 (0.05)
Fe ₂ O ₃	10.80	10.25	11.05	10.37	10.65	10.97	10.90	10.10	12.19	10.78	11.246 (0.09)
MnO	0.09	0.10	0.12	0.11	0.10	0.10	0.13	0.09	0.11	0.17	0.164 (3.02)
MgO	26.30	27.16	26.94	27.12	26.86	26.24	26.67	27.13	26.06	33.88	9.44 (1.80)
CaO	5.00	4.69	3.09	4.38	4.46	4.76	3.54	4.82	4.13	6.05	13.42 (0.95)
Na ₂ O	0.02	0.09	0.00	0.82	0.52	0.05	0.02	0.20	0.01	0.13	1.716 (1.40)
K ₂ O	0.00	0.01	0.00	0.03	0.04	0.01	0.00	0.01	0.02	0.03	0.026 (2.72)
P ₂ O ₅	0.00	0.01	0.01	0.01	0.01	0.01	0.02	0.00	0.02	0.02	0.048 (2.95)
Mg#	83	84	81	84	83	83	83	84	81	86	–
LOI	1.16	1.33	0.62	0.95	1.00	2.02	1.51	1.85	0.93	2.33	–
Cr	1682	2413	2342	2674	2449	1944	2488	2557	1734	2611	375.29 (1.46)
Co	86	76	78	82	74	83	79	76	95	100	52.27 (0.77)
Ni	404	432	429	491	445	388	501	466	403	1425	153.68 (1.45)
Rb	2	2	3	3	4	2	5	3	3	1	0.28 (3.01)
Sr	30	36	36	24	36	19	46	42	26	15	112.48 (0.36)
Cs	0.2	0.1	0.3	0.3	0.6	0.2	0.3	0.1	0.5	0.3	0.00 (7.85)
Ba	45	53	37	95	53	45	64	51	65	10	7.72 (7.01)
Sc	29	29	32	31	34	31	33	29	36	26	43.68 (2.99)
V	129	124	106	113	120	124	116	125	127	143	320.93 (2.36)
Nb	0.52	0.57	0.79	0.76	0.65	1.16	1.14	0.54	0.77	0.42	0.62 (4.05)
Zr	12	16	17	21	14	25	29	13	28	9	15.78 (1.60)
Hf	0.32	0.45	0.46	0.59	0.49	0.65	0.77	0.37	0.78	0.19	0.59 (2.96)
Th	0.19	0.27	0.26	0.27	0.23	0.19	0.28	0.26	0.27	0.04	0.03 (7.21)
Y	6	6	5	7	7	7	8	6	7	5	16.24 (1.06)
La	1.37	1.35	2.04	1.39	1.54	1.21	1.60	2.00	1.87	0.49	0.68 (1.70)
Ce	3.30	3.67	4.08	3.30	3.57	3.15	3.84	4.03	4.34	1.41	2.06 (0.40)
Pr	0.51	0.52	0.52	0.53	0.53	0.52	0.61	0.54	0.61	0.24	0.41 (1.04)
Nd	2.21	2.14	2.09	2.37	2.25	2.37	2.75	2.18	2.54	1.35	2.42 (1.64)
Sm	0.63	0.57	0.51	0.70	0.64	0.67	0.83	0.58	0.67	0.47	1.09 (2.73)
Eu	0.20	0.22	0.17	0.22	0.21	0.19	0.21	0.21	0.19	0.17	0.51 (2.03)
Gd	0.72	0.72	0.63	0.88	0.76	0.83	0.97	0.69	0.81	0.70	1.79 (2.80)
Tb	0.13	0.12	0.12	0.16	0.14	0.14	0.18	0.13	0.14	0.13	0.36 (2.23)
Dy	0.86	0.82	0.76	1.05	0.95	0.95	1.19	0.87	0.96	0.84	2.42 (2.90)
Ho	0.20	0.19	0.18	0.24	0.22	0.22	0.27	0.20	0.22	0.18	0.55 (3.19)
Er	0.62	0.59	0.55	0.71	0.65	0.65	0.81	0.62	0.67	0.52	1.55 (3.19)
Tm	0.10	0.10	0.09	0.12	0.11	0.11	0.13	0.10	0.11	0.07	0.24 (3.42)
Yb	0.70	0.71	0.67	0.83	0.76	0.78	0.94	0.75	0.79	0.48	1.62 (3.61)
Lu	0.12	0.13	0.11	0.13	0.13	0.13	0.15	0.12	0.13	0.07	0.25 (4.07)

4. Results

4.1. Petrography and Mineral Chemistry

The rock is porphyritic in nature and is consistent with the preservation of primary igneous textures (Figure 3a–d). Euhedral to subhedral phenocrysts of pyroxene are noticed in relatively fine grained groundmass (Figure 3a–e). The groundmass is composed of talc (Figure 3f), serpentine, and tremolite. Development of planar fabric is also noticed in the groundmass (Figure 3a,b). In plane polarized light, orthopyroxene exhibits high relief and straight extinction under the crossed nicols. Along the grain margins, orthopyroxene phenocrysts are altered to talc (Figure 3e).

The clinopyroxene is a calcic pyroxene, and mineral chemistry indicates that it is a diopside (Table 1; Figure 4). On the other hand, the orthopyroxene is a low calcic pyroxene, which is compositionally identified as an enstatite (Table 1; Figure 4). The clinopyroxene has been metamorphosed and altered to amphibole in the groundmass and compositionally ranges from tremolite to Mg-hornblende (Table 2). Extremely fine, disseminated grains of Cr-spinel, apatite, rutile, and ilmenite are also present in the groundmass (Table 3). Apatite occurs as euhedral to subhedral prismatic grains that range in size from 40 to 50 µm. Rutile is reddish in colour and it shows high relief. Ilmenite is the opaque Fe–Ti oxide, when observed under high magnification under the reflected light it is anisotropic in nature.

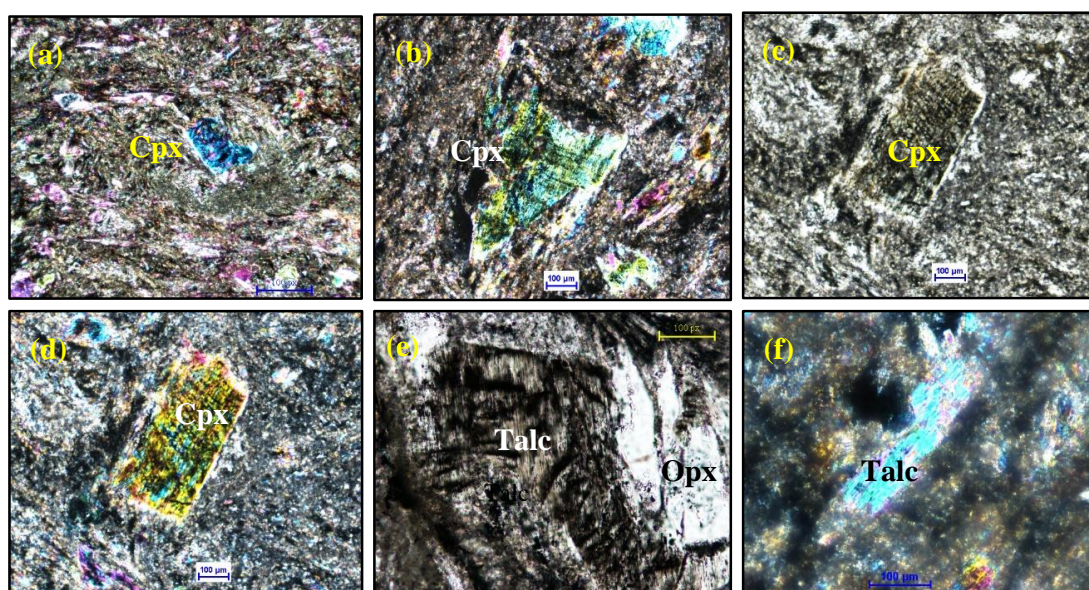


Figure 3. Photomicrographs of Holenarsipur high-Si high-Mg volcanic rocks. The rocks exhibit porphyritic texture with clinopyroxene (a–d), and orthopyroxene (e) in the phenocryst phase, and talc (f) in the groundmass. Note that all the photographs have been taken under uniform magnification of 100 µm. See text for details.

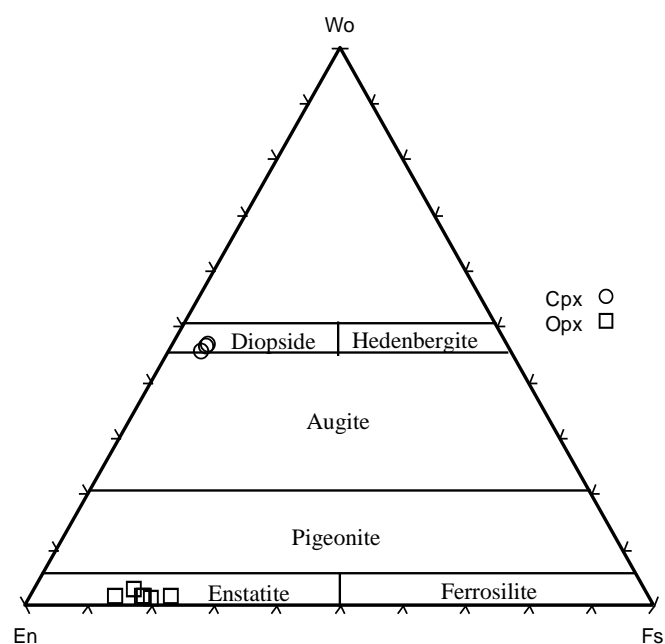


Figure 4. Enstatite–Diopside–Ferrosilite (En–Di–Fs; Morimoto [18]), trilinear diagram for the pyroxene compositions in the Holenarsipur high-Si high-Mg volcanics.

4.2. Bulk-Rock Geochemistry

The rocks consist of high SiO_2 (52–54 wt. %), MgO (~27 wt. %), and Mg\# (~83); and, moderate concentrations of TiO_2 (0.15–0.25 wt. %), Al_2O_3 (3.9–5.0 wt. %) and $\text{Fe}_2\text{O}_3^{(\text{T})}$ (10.1–12.2 wt. %) (Table 4). Trace element abundances indicate moderately high concentrations of compatible elements Cr (1682–2674 ppm) and Ni (388–501 ppm). The rocks are further characterized by high $\text{Al}_2\text{O}_3/\text{TiO}_2$ ratio (19–33) relative to the chondritic value (~22) [17]. Their chondrite normalized REE patterns (Figure 5a,b) have elevated light-REE when compared to the middle-REE ($\text{La}_\text{N}/\text{Sm}_\text{N} = 1.1\text{--}2.5$), slightly

negative Eu anomalies, and depletions in the middle-REE relative to the heavy-REE ($Gd_N/Yb_N = 0.77\text{--}0.88$) resulting in concave-up REE patterns. In a primitive mantle-normalized trace element variation diagram (Figure 5d,e), the samples display prominent negative Nb anomaly with $(Nb/La)_{pm}$ and $(Nb/Th)_{pm} < 1$; negative Ti, i.e., $(Ti/Gd)_{pm} = 0.45\text{--}0.83$, and generally positive Zr anomaly, i.e., $(Zr/Sm)_{pm} = 0.76\text{--}1.65$, with near chondritic Zr/Hf ~ 36 .

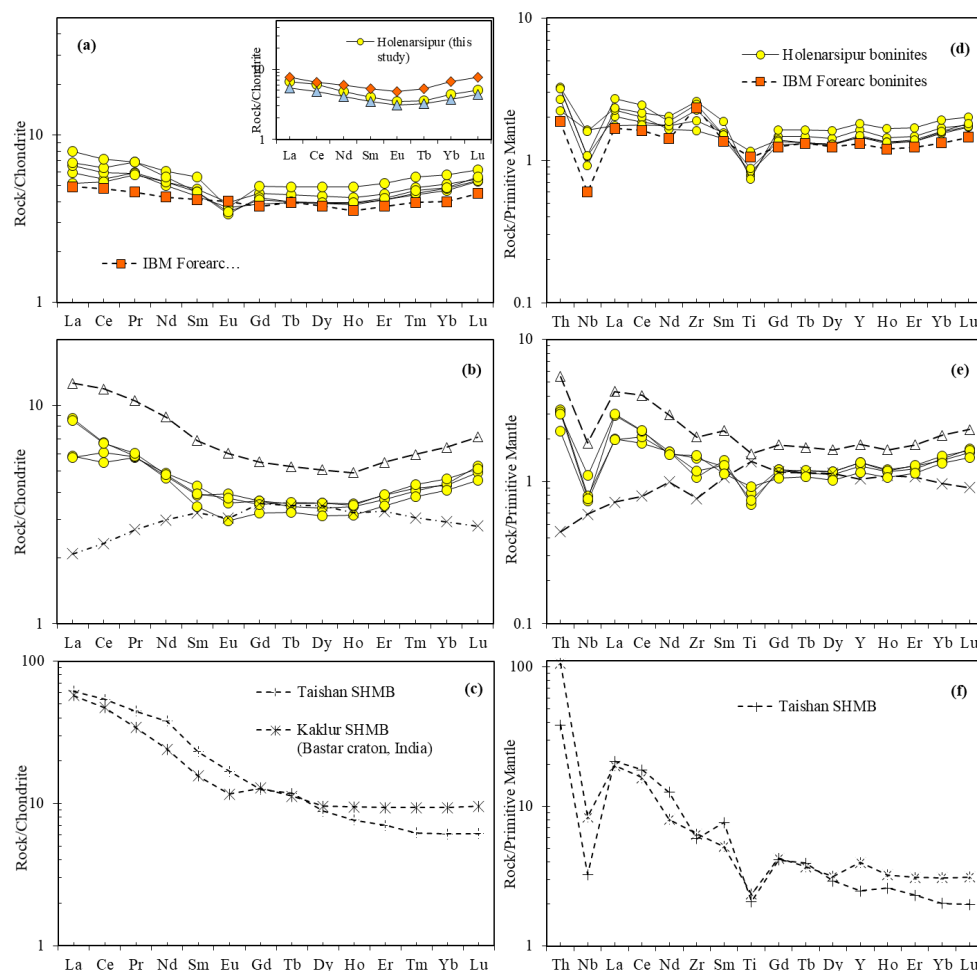


Figure 5. Chondrite normalized rare earth element (REE) patterns (a–c); and, (d–f) primitive mantle normalized trace element variation diagrams. Chondrite and primitive mantle values are from Sun and McDonough [17]. Data for Izu-Bonin-Mariana fore arc boninites in (a,d) is from Reagen et al. [2]. The REE patterns of the Phanerozoic boninites in (a) are plotted from Hickey and Frey [1], and shown for comparison. The data for Whundo boninites shown in (b,e) is from Smithies et al. [6]. Note the identical nature of the normalized REE and trace element patterns exhibited by the ~ 3.3 Ga Holenarsipur high-Si high-Mg volcanics in comparison to the ~ 3.1 Ga Whundo boninites. The patterns are converse to that displayed by the Kadihalli komatiites (Table 4) [13]. The Neoproterozoic siliceous high-Mg basalts in (c,f) Srivastava and Singh [19] and Peng et al. [20] are also shown for comparison. See text for details.

5. Discussion

5.1. Classification

The SiO_2 contents in the Holenarsipur volcanics are consistent with a basaltic andesite composition [21]. The MgO contents, however, are significantly higher when compared to the basaltic andesites. In the revised geochemical classification scheme of Le Bas [21] proposed for high-Mg volcanic rocks, the Holenarsipur volcanics with high silica and magnesium, and low titanium contents

are classified as boninites ($\text{MgO} > 8 \text{ wt. } \%$, $\text{TiO}_2 < 0.5 \text{ wt. } \%$, and $\text{SiO}_2 > 52 \text{ wt. } \%$; Figure 6a). Taking into account of the physio-chemical conditions that the belt may have endured through the Mesoarchean until the present, it is a potential possibility that the silica and alkali contents in these rocks could have been affected by alteration and metamorphism during post-magmatic crystallization processes; therefore, we adopted the classification scheme that was proposed by Hanski et al. [22]. The diagram Al_2O_3 vs. TiO_2 (Figure 6b) discriminates between boninites, komatiites, and their variants, picrites, and meimechite. The Holenarsipur samples plot in the boninite field, and few samples toggle the boundary between Al-depleted komatiite and boninite field (Figure 6b). On the basis of $\text{CaO}/\text{Al}_2\text{O}_3$ ratio (>0.75), Crawford et al. [23] divided the boninites into distinct low-Ca and high-Ca types. The high-Ca type are further characterized by $\text{SiO}_2 < 56 \text{ wt. } \%$ and crystallize both high- and low-Ca pyroxene, along with olivine as phenocryst phase. By analogy, the Holenarsipur boninites conform to the above mineralogical and geochemical criteria, and hence, resemble high-Ca type boninites.

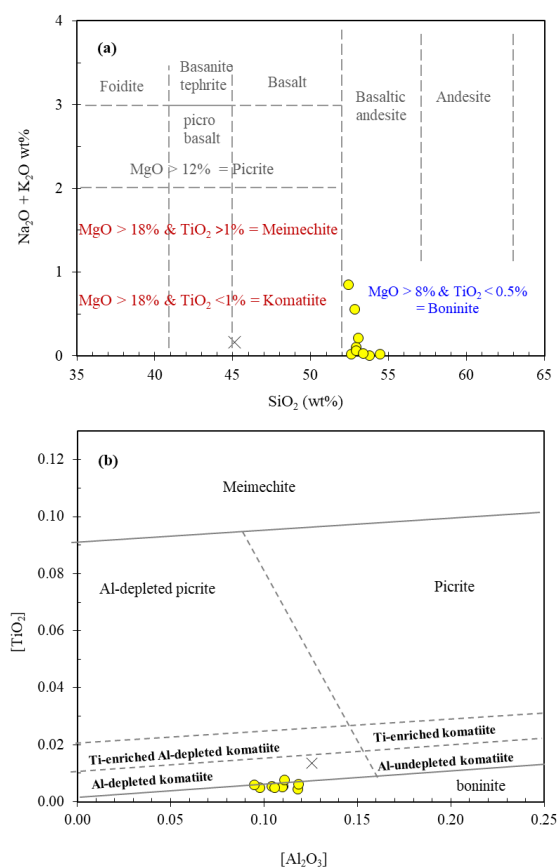


Figure 6. (a) SiO_2 vs. $(\text{Na}_2\text{O} + \text{K}_2\text{O})$ classification diagram for high-Mg volcanics, after Le Bas [21]; (b) Al_2O_3 vs. TiO_2 classification diagram adopted from Hanski et al. [22]. On the basis of above classification schemes, the Holenarsipur high-Si high-Mg volcanic rocks have been identified as boninites. Symbols are same as in Figure 5. See text for details.

5.2. Alteration and Crustal Contamination

In hydrothermally altered ultramafic rocks, talc is a common alteration phase, e.g., [24]. Simultaneous addition of silica and removal of magnesium in conjunction with CO_2 addition during serpentinization can also result in the formation of talc, e.g., [25]. In such a case, talc often coexists with carbonate minerals, e.g., magnesite or dolomite or calcite. The petrographic observations, however, do not indicate the coexistence of carbonate minerals in the Holenarsipur boninites. Therefore, we presume that the precursor rocks were subjected to purely hydrothermal alteration, resulting in the formation of serpentine, talc, and amphibole replacing olivine, orthopyroxene, and clinopyroxene, respectively.

The rocks are characterized by uniform major and trace element compositions, and their interelement ratios. They have a narrow range in their Th/Ce \sim 0.07, Nb/Zr \sim 0.04, Zr/Hf \sim 37 ratios. Although the REE patterns appear to be coherent (Figure 5a,b), slight negative Eu anomalies in some of the samples, as well as the absence of Eu anomaly in the rest, is taken to reflect variably altered nature of the samples. The high MgO, Mg#, Cr, and Ni contents, very low abundance in incompatible elements that are typically enriched in the crust (K, Na, Rb, Ba), as well as low high field strength elements (HFSE; Zr, Nb, Y) and REE concentrations in these rocks are inconsistent with modification by assimilation of Archean upper continental crust. Contamination of pristine magma by assimilation of crustal material en route to the surface will result in significantly lower Nb/Th ratio [26] in the erupted melt when compared to the primary mantle derived melt. As there is evidence for the presence of the Mesoarchean upper crust in the western Dharwar craton [12], to first order, the negative Nb anomalies relative to the REE, i.e., (Nb/La)_{pm} < 1 in the Holenarsipur boninites, may then reflect a crustal contamination signature. The rocks, however, in contrast to the relatively high Nb (\sim 7 ppm) combined with high La/Nb as observed in the Holenarsipur TTG [12], do not plot on an imaginary mixing line between the average N-MORB and the Mesoarchean continental crust in the study area (Figure 7A), as would be expected in case of crustally contaminated boninites (Figure 7A; [27]). The rocks, instead display increasing La/Nb ratio with decreasing Nb content (Figure 7A).

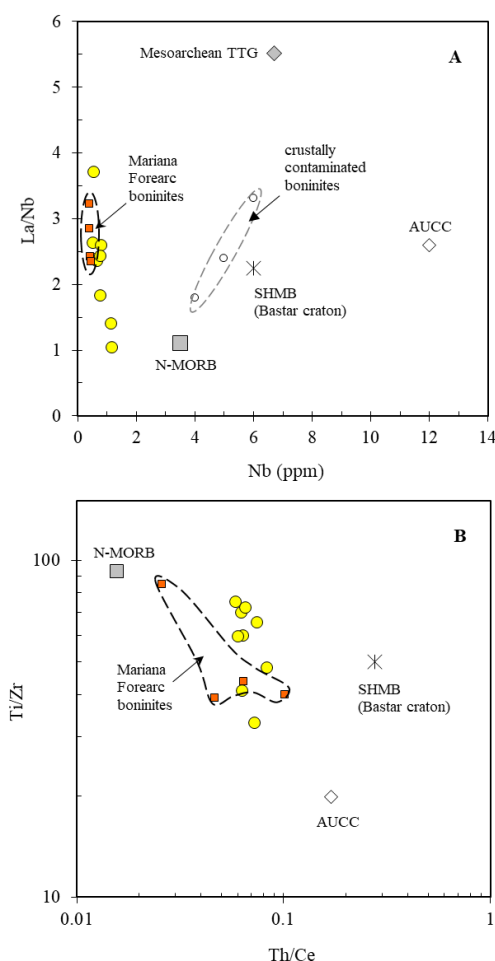


Figure 7. (A) Nb vs. La/Nb; and, (B) Th/Ce vs. Ti/Zr, bivariate diagrams for the Holenarsipur boninites. Data for Izu-Bonin-Mariana fore arc boninites is from Reagen et al. [2]. Values for N-MORB [28], Archean Upper Continental Crust (AUCC; [29]), crustally contaminated boninites [27], siliceous high-Mg basalts (SHMB; [19]) and Mesoarchean TTG from the Holenarsipur [12], are also shown for comparison. See text for details.

Moreover, when a mantle derived magma assimilates the preexisting felsic crustal material, the composition of the melt is enriched in Zr and Th, and consequently, it produces a low Ti/Zr and high Th/Ce signature that is similar to that observed in the Archean upper continental crust (Figure 7B; Ti/Zr ~20 and Th/Ce ~0.17; [29]). Although pristine boninite magmas generated in the intraoceanic settings exhibit a wide range in their Ti/Zr ratios from 23 to 85 [1,2], the Th/Ce ratio, however, remains ≤ 0.1 and is inconsistent with any crustal assimilation. Accordingly, we interpret the low Th/Ce and comparatively high Ti/Zr ratios in the Holenarsipur boninites to represent pristine magmatic compositions (Figure 7B). Further, the interelement ratios involving the incompatible elements Th-Nb-Yb in the Holenarsipur boninites are consistent with a subduction-related volcanic arc signature (Figure 8). Accordingly, we infer that the geochemical attributes of the Holenarsipur boninites are inconsistent with any interaction with the Mesoarchean upper continental crust regionally preserved in the study area, and hence, they were presumably generated in a subduction-related intraoceanic arc setting.

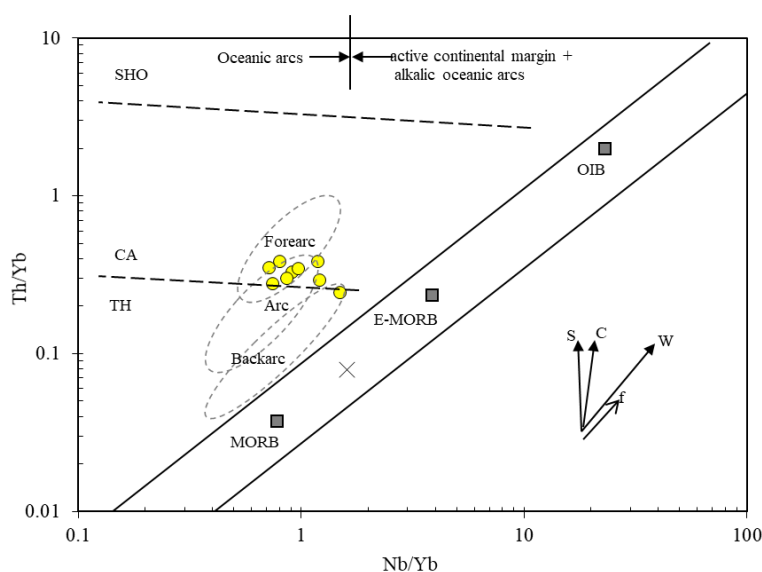


Figure 8. Tectonic discrimination diagram of Nb/Yb vs. Th/Yb after Pearce [30]. The dashed field boundaries for TH = tholeiitic, CA = calc-alkaline, and SHO = shoshonitic rocks are from convergent margins. The bold arrows in the bottom right are S = subduction component, C = crustal contaminant component, W = within plate, and f = fractional crystallization vectors. The Holenarsipur boninites plot sub-parallel to the terrestrial MORB–OIB array, and within the Phanerozoic arc fields. The Phanerozoic arc, fore-arc, and back-arc basalt fields are from Metcalf and Shervais [31]. Symbols are same as in Figure 5. See text for details.

5.3. Comparison with Komatiites and Siliceous High-Mg Basalts (SHMB)

The high MgO and Mg# in combination with low Al_2O_3 , CaO, and TiO_2 concentrations, and extremely low HFSE (Nb, Zr, Y) and Yb in the Holenarsipur boninites, to first order, resemble Al-depleted komatiites, for example, komatiites in the Kadihalli area in the western Dharwar craton (Figure 1a; Table 4; [13]). However, the Holenarsipur boninites do not have any textural attributes of a komatiite. The high MgO contents may be due to second stage partial melting of a refractory and depleted mantle source [32]. In comparison to the Holenarsipur boninites, the Al-depleted Kadihalli komatiites rather exhibit remarkable contrasting chondrite normalized rare earth element patterns with a hump-shaped (convex-shaped) middle-REE, relative to the light-REE and the heavy-REE producing inverted concave-up patterns (Figure 5b). Moreover, the arc magmatic signature involving negative Nb and Ti anomalies (Figure 5d,e) in the Holenarsipur boninites are in stark contrast to the Kadihalli komatiites that are characterized by positive Nb and Ti anomalies, and plot within the

terrestrial MORB-mantle array, as consistent with a non-subduction related origin (Figure 8). Further, the komatiites, including Al-depleted and Al-undepleted type e.g., Chavagnac [33], are characterized by low SiO_2 (<52 wt. %), sub to near chondritic $\text{Al}_2\text{O}_3/\text{TiO}_2$, and Ti/Sc ratios, and $(\text{Gd}/\text{Yb})_N \geq 1$; which contrasts the higher SiO_2 and $\text{Al}_2\text{O}_3/\text{TiO}_2$, and essentially sub-chondritic Ti/Sc and $(\text{Gd}/\text{Yb})_N$ ratios in the Holenarsipur boninites (Figure 9). Furthermore, as in the case of boninites, orthopyroxene is not a ubiquitous phase in the komatiite melts. In komatiite cumulates, however, they have been identified from the Abitibi belt [34]. The clinopyroxene is predominantly an augite or sub-calcic augite that occurs in a komatiite melt [35].

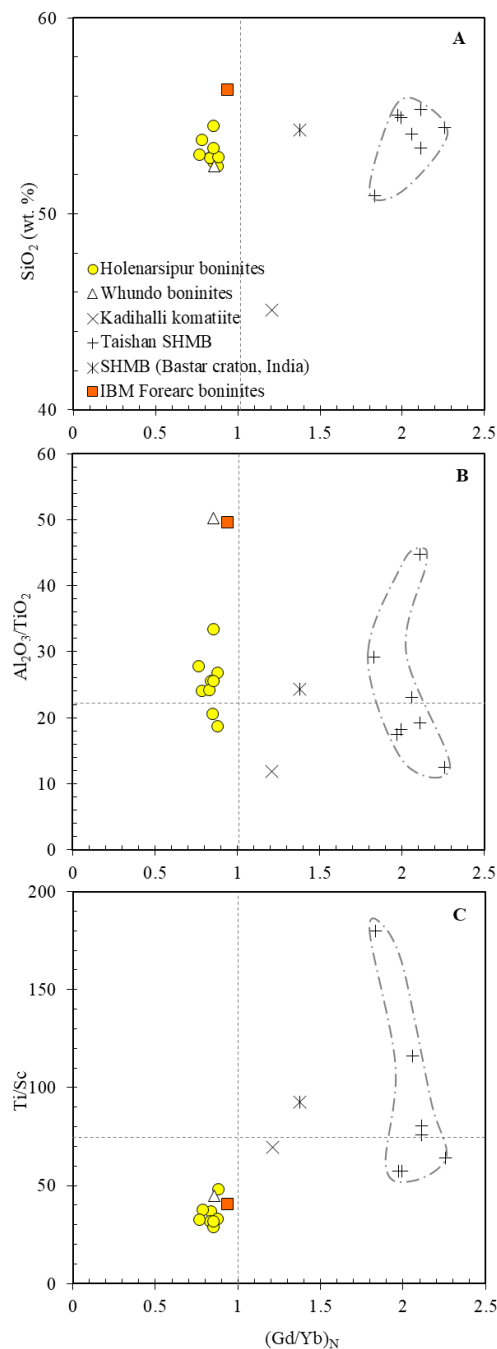


Figure 9. Chondrite normalized (Gd/Yb) ratio vs. (A) SiO_2 ; (B) $\text{Al}_2\text{O}_3/\text{TiO}_2$; and, (C) Ti/Sc bivariate diagrams to discriminate between the boninites, and komatiites and siliceous high-Mg basalts. Stippled lines are chondrite values [17]. Data sources as in Figure 5. See text for details.

The high SiO₂ contents in combination with high MgO in the Holenarsipur boninites are comparable to the siliceous high-Mg basalts (SHMB), which generally occur in the granite-greenstone terranes near the Archean-Proterozoic boundary [20]. As such, SHMB have not been identified in the Dharwar craton. Although, it is widely accepted that SHMB are the products of crustal assimilation and fractional crystallization (AFC) of a komatiite magma [36,37], their origin remains enigmatic. The ~2.54 Ga Taishan SHMB in the North China Craton are characterized by pristine Nd isotopic compositions. They were interpreted as the products of the partial melting of a subduction modified mantle source, and not due to the AFC of a komatiite magma [20]. Nevertheless, the crustally uncontaminated Holenarsipur boninites can be readily distinguished from the SHMB (Figure 5c,f), by their concave-up REE patterns and reversely fractionated heavy-REE resulting in (Gd/Yb)_N < 1 (Figure 9).

5.4. Petrogenetic Implications

The Holenarsipur boninites consist of orthopyroxene and clinopyroxene phenocrysts with serpentine and talc that were derived from altered olivine and orthopyroxene, respectively, in the groundmass. This suggests that the unaltered protolith consisted of olivine plus Cr-spinel plus orthopyroxene plus clinopyroxene, which is consistent with the mineralogical composition that is typically observed in the Phanerozoic high-calcic boninites [38]. This further indicates that the source peridotite had a spinel lherzolite composition.

As discussed earlier, crustal contamination is reasonably ruled out and it cannot account for the unique trace element attributes that were observed in the Holenarsipur boninites, which are typically characterized by low TiO₂ (0.15–0.25 wt. %; avg. 0.18 wt. %), Al₂O₃ (3.9–5.0 wt. %; avg. 4.5 wt. %) and CaO (3.5–5.0 wt. %; avg. 4.3 wt. %) contents. Their Al₂O₃/TiO₂ (19–33; avg. 25) and CaO/TiO₂ (15–33; avg. 24) ratios extend to higher than chondritic values (22 and 18, respectively; [17]), which imply their derivation from a refractory mantle source. Further evidence for the refractory nature of the mantle source is indicated by high Cr# ((Cr/Cr + Al) = 0.8) in the Cr-spinel, which is disseminated as extremely minute grains in the groundmass. The high MgO, Mg#, Cr, and Ni contents, low Nb, Zr, Y, and their interelement ratios Zr/Y (~3) and Nb/Y (~0.12), and extremely low total REE abundance (~12 ppm) in combination with the primitive mantle normalized negative Nb and Ti anomalies relative to the neighbouring REE further suggest that the melts were produced from relatively high degree partial melting of a refractory and depleted peridotitic mantle source.

The enrichment in the light-REE (La_N/Sm_N) does not correlate with the abundances of Th, Zr, Sr, and Ba, which would otherwise reflect contribution from sedimentary sources [12]. Alternatively, the subtle enrichment in Th, Zr, and the light-REE (La_N/Sm_N = 1.8–4.0; avg. 2.6) indicate that the refractory and prior depleted mantle source was subsequently metasomatized by the fluids/melts derived from the sub-arc mantle generated from the dehydration of altered oceanic crust, shortly prior to, or during, the melt generation process. The ornate REE patterns that were exhibited by the Holenarsipur boninites are identical to those that were observed in the Tertiary boninites from the Bonin Islands and the Mariana Trench (Figure 5a; [1]), and the primitive mantle normalized trace element patterns are identical to the IBM fore-arc boninites (Figure 5b; [2]). Although, SiO₂, TiO₂, Al₂O₃, and CaO contents in the Holenarsipur boninites are similar to the Phanerozoic boninites, the MgO contents are relatively high (MgO = 26 wt. % vs. 19 wt. % [39]), but possess similar mineralogical composition and identical high Mg# (~83). Therefore, we infer that the Holenarsipur boninites represent near primary magmas that were derived from high degree partial melting of a peridotitic mantle source.

Besides the boninitic rocks reported here from the ~3.3 Ga Holenarsipur greenstone belt, boninite-like rocks have also been recognized in the greenstone terranes of Eo-, Meso- and Neoproterozoic age [5–8,16]. The origin of boninites, in general, is attributed to a two stage melting process involving depletion of a mantle source due to prior melt extraction events, presumably at a mid-oceanic ridge, in the first stage, followed by partial melting of this depleted source triggered by the fluids/melts derived from the dehydration of subducted altered oceanic crust in the sub-arc mantle, in the second

stage. The documentation of boninites throughout the Archean, importantly indicates that the geodynamic process that was involved in the generation of Archean boninites, was perhaps not any significantly different from the widely recognized two-stage melt generation process that produced the Phanerozoic boninites, and hence, provides compelling evidence for the onset of Phanerozoic type plate tectonic processes at least by ~3.3 Ga, in the Earth's evolutionary history.

6. Conclusions

We present detailed field, petrography, and geochemistry of the newly identified high-Si high-Mg volcanic rocks from the ~3.3 Ga Holenarsipur greenstone belt that are identical to the Phanerozoic boninites. The geochemical attributes are consistent with the generation of the Holenarsipur boninites from a refractory and prior depleted peridotitic mantle source in a subduction-related intraoceanic arc setting in the Paleoproterozoic. This new finding essentially bridges the gap between the late Eoarchean [5] and the early Mesoproterozoic [6], and it provides convincing evidence for the persistence of subduction-related plate tectonic processes throughout the Archean during the Earth's early evolutionary history.

Author Contributions: The idea has been conceived and conceptualized by T.C.K.; A.K.K. and T.C.K. developed the analytical methodology for the analysis of major element oxides in fused glass beads using WD-XRF; V.V.S.S. and M.M.K. conducted petrographic studies and provided formal analysis of the samples using EPMA; Field investigations were carried out by T.C.K., S.H.J. and V.V.S.S.; Writing and preparation of the original draft manuscript was done by T.C.K.

Funding: This research was funded by an inhouse project of CSIR-NGRI grant number [MLP-6201-28 (CM) & MLP-6406-28 (CM)].

Acknowledgments: Authors are thankful to Virendra Mani Tiwari, the Director NGRI, for permission [NGRI/Lib/2018/pub-54] to publish this work. Manavalan Satyanarayanan and Saripoot Sawant are thanked for trace element analysis by HR-ICP-MS. Ismail Mohammed Younnis is much appreciated for his assistance in the wet chemistry lab.

Conflicts of Interest: The authors declare no conflict of interest. Furthermore, the funders had no role in the design of the study; in the collection, analyses, or interpretation of data; in the writing of the manuscript, and in the decision to publish the results.

References

1. Hickey, R.L.; Frey, F.A. Geochemical characteristics of boninite series volcanics: Implications for their source. *Geochim. Cosmochim. Acta* **1982**, *46*, 2099–2115. [[CrossRef](#)]
2. Reagan, M.K.; Ishizuka, O.; Stern, R.J.; Kelley, A.K.; Ohara, Y.; Blichert-Toft, J.; Bloomer, S.H.; Cash, J.; Fryer, P.; Hanan, B.B.; et al. Fore-arc basalts and subduction initiation in the Izu-Bonin-Mariana system. *Geochem. Geophys. Geosyst.* **2010**, *11*, Q03X12. [[CrossRef](#)]
3. Beccaluva, L.; Serri, G. Boninitic and low-Ti subduction-related lavas from intraoceanic arc-back-arc systems and low-Ti ophiolites: A reappraisal of their petrogenesis and original tectonic setting. *Tectonophysics* **1988**, *146*, 291–315. [[CrossRef](#)]
4. Bedard, J.H. Petrogenesis of boninites from the Betts Cove ophiolite, Newfoundland, Canada: Identification of subducted source components. *J. Petrol.* **1999**, *40*, 1853–1889. [[CrossRef](#)]
5. Polat, A.; Hofmann, A.W.; Rosing, M. Boninite-like volcanic rocks in the 3.7–3.8 Ga Isua greenstone belt, West Greenland: Geochemical evidence for intra-oceanic subduction zone processes in the Earth. *Chem. Geol.* **2002**, *184*, 231–254. [[CrossRef](#)]
6. Smithies, R.H.; Champion, D.C.; Van Kranendonk, N.J.; Howard, H.M.; Hickman, A.H. Modern style subduction processes in the Mesoproterozoic: Geochemical evidence from the 3.12 Ga Whundo intra-oceanic arc. *Earth Planet. Sci. Lett.* **2005**, *231*, 221–237. [[CrossRef](#)]
7. Manikyamba, C.; Naqvi, S.M.; Subba Rao, D.V.; Ram Mohan, M.; Khanna, T.C.; Rao, T.G.; Reddy, G.L.N. Boninites from the Neoproterozoic Gadwal greenstone belt, eastern Dharwar craton, India: Implications for Archean subduction processes. *Earth Planet. Sci. Lett.* **2005**, *230*, 65–83. [[CrossRef](#)]

8. Khanna, T.C.; Bizimis, M.; Yogodzinski, G.M.; Mallick, S. Hafnium-neodymium isotope systematics of the 2.7 Ga Gadwal greenstone terrane, eastern Dharwar craton, India: Implications for the evolution of the Archean depleted mantle. *Geochim. Cosmochim. Acta* **2014**, *127*, 10–24. [[CrossRef](#)]
9. Peucat, J.-J.; Bouhallier, H.; Fanning, C.M.; Jayananda, M. Age of Holenarsipur schist belt, relationships with the surrounding gneisses (Karnataka, South India). *J. Geol. Soc. India* **1995**, *103*, 701–710.
10. Swami Nath, J.; Ramakrishnan, M. The early Precambrian supracrustals of southern Karnataka. *Mem. Geol. Surv. India* **1981**, *112*, 1–350.
11. Naqvi, S.M.; Rogers, J.J.W. Precambrian geology of India. *Oxf. Monogr. Geol. Geophys.* **1987**, *6*, 1–233.
12. Naqvi, S.M.; Ram Mohan, M.; Rana Prathap, J.G.; Srinivasa Sarma, D. Adakite–TTG connection and fate of Mesoarchean basaltic crust of Holenarsipur Nucleus, Dharwar Craton, India. *J. Asian Earth Sci.* **2009**, *35*, 416–434. [[CrossRef](#)]
13. Jaffri, S.H.; Subba Rao, D.V.; Ahmad, S.M.; Mathur, R. Spinifex textured peridotitic komatiite from Nuggihalli and H.N. Pur schist belts, Karnataka. *J. Geol. Soc. India* **1997**, *49*, 33–38.
14. Keshav, A.K.; Khanna, T.C.; Rama Mohan, K. Rapid quantitative determination of major and trace elements in silicate rocks and soils employing fused glass discs using wavelength dispersive X-ray fluorescence spectrometry. *Spectrochim. Acta Part B* **2016**, *122*, 165–171.
15. Khanna, T.C.; Sessa Sai, V.V.; Bizimis, M.; Keshav Krishna, A. Petrogenesis of Basalt–high-Mg Andesite–Adakite in the Neoproterozoic Veligallu Greenstone Terrane: Geochemical evidence for a rifted back-arc crust in the eastern Dharwar craton, India. *Precamb. Res.* **2015**, *258*, 260–277. [[CrossRef](#)]
16. Khanna, T.C.; Sessa Sai, V.V.; Bizimis, M.; Keshav Krishna, A. Petrogenesis of ultramafics in the Neoproterozoic Veligallu greenstone terrane, eastern Dharwar craton, India: Constraints from bulk-rock geochemistry and Lu–Hf isotopes. *Precamb. Res.* **2016**, *285*, 186–201. [[CrossRef](#)]
17. Sun, S.S.; McDonough, W.F. Chemical and isotopic systematics of oceanic basalts: Implications for mantle compositions and processes. In *Magmatism in Ocean Basins*; Saunders, A.D., Norry, M.J., Eds.; Geological Society Special Publication: London, UK, 1989; Volume 42, pp. 313–345.
18. Morimoto, N. Nomenclature of Pyroxenes. *Mineral. Petrol.* **1988**, *39*, 55–76. [[CrossRef](#)]
19. Srivastava, R.K.; Singh, R.K. Petrology and geochemistry of the late Archean siliceous high-Mg basalts (SHMB) from Kaklur, southern Bastar craton, Central India. *J. Geol. Soc. India* **1999**, *53*, 693–704.
20. Peng, T.; Wilde, S.A.; Fan, W.; Peng, B. Neoproterozoic siliceous high-Mg basalt (SHMB) from the Taishan granite–greenstone terrane, Eastern North China Craton: Petrogenesis and tectonic implications. *Precamb. Res.* **2013**, *228*, 233–249. [[CrossRef](#)]
21. Le Bas, M.J. IUGS reclassification of the high-Mg and picritic volcanic rocks. *J. Petrol.* **2000**, *41*, 1467–1470. [[CrossRef](#)]
22. Hanski, E.J.; Huhma, H.; Rastas, P.; Kamenetsky, V.S. The Palaeoproterozoic komatiite–picrite association of Finnish Lapland. *J. Petrol.* **2001**, *42*, 855–876. [[CrossRef](#)]
23. Crawford, A.J.; Fallon, T.J.; Green, D.H. Classification, petrogenesis and tectonic setting of boninites. In *Boninites and Related Rocks*; Crawford, A.J., Ed.; Unwin Hyman: London, UK, 1989; pp. 1–49.
24. Pawley, A.R.; Wood, B.J. The high-pressure stability of talc and 10Å phase: Potential storage sites for H₂O in subduction zones. *Am. Mineral.* **1995**, *80*, 998–1003. [[CrossRef](#)]
25. Naldrett, A.J. Talc–Carbonate alteration of some serpentinitized ultramafic rocks of Timmins, Ontario. *J. Petrol.* **1966**, *7*, 489–499. [[CrossRef](#)]
26. Jochum, K.P.; Arndt, N.T.; Hofmann, A.W. Nb–Th–La in komatiites and basalts: Constraints on komatiite petrogenesis and mantle evolution. *Earth Planet. Sci. Lett.* **1991**, *107*, 272–289. [[CrossRef](#)]
27. Hatton, C.J.; Sharpe, M.R. Significance and origin of boninite-like rocks associated with the Bushveld complex. In *Boninites and Related Rocks*; Crawford, A.J., Ed.; Unwin Hyman: London, UK, 1989; pp. 174–207.
28. Hofmann, A.W. Chemical differentiation of the Earth: The relationship between mantle, continental crust, and oceanic crust. *Earth Planet. Sci. Lett.* **1988**, *90*, 297–314. [[CrossRef](#)]
29. Rudnick, R.L.; Gao, S. Composition of the continental crust. *Treatise Geo-Chem.* **2004**, *3*, 1–64.
30. Pearce, J.A. Geochemical fingerprinting of oceanic basalts with applications to ophiolite classification and the search for Archean oceanic crust. *Lithos* **2008**, *100*, 14–48. [[CrossRef](#)]

31. Metcalf, R.V.; Shervais, J.W. Suprasubduction-zone ophiolites: Is there really an ophiolites conundrum? In *Ophiolites, Arcs, and Batholiths: A Tribute to Cliff Hopson*; Geological Society of America Special Paper; Wright, J.E., Shervais, J.W., Eds.; Geological Society of America: Boulder, CO, USA, 2008; Volume 438, pp. 191–222.
32. Szilas, K.; Naeraa, T.; Schersten, A.; Stendal, H.; Frei, R.; van Hinsberg, V.J.; Kokfelt, T.F.; Rosing, M.T. Origin of Mesoarchean arc-related rocks with boninite/komatiite affinities from southern West Greenland. *Lithos* **2012**, *144–145*, 24–39. [[CrossRef](#)]
33. Chavagnac, V. A geochemical and Nd isotopic study of Barberton komatiites (South Africa): Implication for the Archean mantle. *Lithos* **2004**, *75*, 253–281. [[CrossRef](#)]
34. Arndt, N.T. Thick, layered peridotite-gabbro lava flows in Munro Township, Ontario. *Can. J. Earth Sci.* **1977**, *14*, 2620–2637. [[CrossRef](#)]
35. Cameron, W.E.; Nisbet, E.G.; Dietrich, V.J. Boninites, komatiites and ophiolitic basalts. *Nature* **1979**, *280*, 550–553. [[CrossRef](#)]
36. Arndt, N.T.; Jenner, G.A. Crustally contaminated komatiites and basalts from Kambalda, Western Australia. *Chem. Geol.* **1986**, *56*, 229–255. [[CrossRef](#)]
37. Sun, S.-S.; Nesbitt, R.W.; McCulloch, M.T. Geochemistry and petrogenesis of Archaean and early Proterozoic siliceous high-magnesian basalts. In *Boninites and Related Rocks*; Crawford, A.J., Ed.; Unwin Hyman: London, UK, 1989; pp. 148–173.
38. Falloon, T.J.; Crawford, A.J. The petrogenesis of high-calcium boninite lavas dredged from the northern Tonga ridge. *Earth Planet. Sci. Lett.* **1991**, *102*, 375–394. [[CrossRef](#)]
39. Cameron, W.E. Contrasting boninite-tholeiite associations from New Caledonia. In *Boninites and Related Rocks*; Crawford, A.J., Ed.; Unwin Hyman: London, UK, 1989; pp. 314–338.



© 2018 by the authors. Licensee MDPI, Basel, Switzerland. This article is an open access article distributed under the terms and conditions of the Creative Commons Attribution (CC BY) license (<http://creativecommons.org/licenses/by/4.0/>).